

## Diffuse x-ray scattering from 311 defects in Si

K. Nordlund

Accelerator Laboratory, P.O. Box 43, FIN-00014 University of Helsinki, Finland

(April 22, 2015)

311 defects are extended, rod-like defects which play a central role in the processing of Si during integrated circuit manufacturing. Diffuse x-ray scattering techniques provide a non-destructive means to detect defects in solids. However, to date there has been no knowledge of what the x-ray scattering pattern from 311 defects looks like. Using a recently introduced fully atomistic modeling scheme, I calculate the diffuse x-ray scattering patterns from 311 defects. The results demonstrate how 311 defects can be detected, how the main varieties of 311 defect can be distinguished, and how both the defect width and length can be derived from the scattering.

PACS numbers: 61.72.Dd, 61.72.Nn, 61.82.Fk, 61.80.Jh

### I. INTRODUCTION

When the damage produced by ion implantation of Si is annealed, several types of interstitial-like defects are present in the implanted region<sup>1</sup>. The vast majority of these defects have to be removed in order to produce working semiconductor devices, so the properties of these defects are of great interest. The most important extended defects are so called “311” defects, stacking faults, and perfect dislocation loops. Although all of these defects can be detected using transmission electron microscopy (TEM), it would be beneficial to have complementary, preferably non-destructive means to detect the same defects. Diffuse X-ray diffraction methods can be used as such a method<sup>2-6</sup>.

Although the basic theory of diffuse x-ray scattering from defects is well established<sup>7</sup>, applying this theory to extended defects is not straightforward. The numerical calculations of Ehrhart *et al.*<sup>8</sup> predict the x-ray scattering for two of the aforementioned three defect types, i.e. stacking faults and perfect dislocation loops. However, to my knowledge there are no calculations of the nature of the diffuse x-ray scattering from 311 defects. The likely reason to this is the complicated nature of these defects<sup>9-13</sup>. TEM experiments show that they have the form of interstitial platelets, with widths of typically 10 - 1000 Å, and lengths which can be of the order of microns (because of the large aspect ratio, the defects are also often called “rod-like”). The platelets are observed on {311} lattice planes, which gives the defects their name. In the platelet, the extra atoms lie in configurations containing 5-, 7- and 8-membered atom rings, whereas perfect Si only contains 6-membered rings. However, in a perfect 311 defect all Si atoms still have exactly 4 bonds (as in perfect Si), which makes the defects very stable.

To calculate the x-ray scattering from 311 defects, I use a recently developed fully atomistic modeling scheme to obtain the x-ray scattering<sup>14,15</sup>. This scheme enables prediction of the x-ray scattering for any defect for which an atomic configuration is known, although computer capacity currently limits the method to defects with sizes at most of the order of 100 Å.

Here I use the method to calculate the scattering for the two configurations of 311 defects which are believed

to be the most abundant ones in experiments, the “1HeXZD” and “IRD” defects<sup>11</sup>.

### II. METHOD

#### A. Calculation of x-ray scattering

The atomistic calculation scheme used here has been presented in detail in Refs. 14, 15, and been shown to be useful in analyzing experimental results on defects in semiconductors<sup>6,16</sup>. Hence I describe here only the most central features and the aspects which are specific to the present study.

To obtain the x-ray scattering for a defect, the coordinates of the defect atoms and atoms in the immediate vicinity are embedded into a large (in this paper normally 600 Å in diameter) sphere of atoms at perfect lattice sites<sup>15</sup>. The coordinates of all the atoms are then relaxed to the closest potential energy minimum using an optimized conjugate gradient scheme. The relaxation gives realistic coordinates of atoms  $R_i$  describing the strain field surrounding the defect. To ensure that the choice of the potential energy model does not affect the result, I did some calculations with two different interatomic potential models<sup>17,18</sup>. No significant difference in the scattering shapes or intensities were observed.

The x-ray scattering within the kinematical approximation is obtained by straightforward summation,

$$S(\mathbf{K}) = N(\sigma/a) \left| f_{\mathbf{K}} \sum_i e^{-\sigma^2 \mathbf{R}_i^2 / 2a^2} e^{i\mathbf{K} \cdot \mathbf{R}_i} \right|^2, \quad (1)$$

Here  $\mathbf{K}$  is a reciprocal lattice vector,  $\mathbf{R}_i$  the atom position,  $a$  the lattice constant,  $f_{\mathbf{K}}$  the atomic form factor, and  $N(\sigma/a)$  a normalization factor. When the interest is only in the qualitative shape of the scattering pattern, one can set  $f = 1$  and  $N = 1$ . To make the results comparable to x-ray experiments (which usually measure the average over a very large number of defects), I average the scattering over all equivalent orientations of the defect in the crystal.

The convolution factor  $\exp(-\sigma^2 \mathbf{R}_i^2 / 2a^2)$  has the effect of broadening the x-ray scattering somewhat. This

complicates quantitative comparison of scattering intensities with experiments. By using a normalizing factor  $N(x) = \sqrt{2}x^3/(4\pi\sqrt{\pi})$  the three-dimensional integral of the Bragg peaks becomes independent of  $\sigma$  (since the Bragg peak is practically symmetric about the maximum, this integral can be evaluated from a one-dimensional scan over the peak). But I found that the integral over the diffuse scattering intensity still may depend on  $\sigma$ , probably because the convolution factor can affect the complex streak patterns obtained in this work in a different manner from that of the Bragg peaks. But if the resolution of the experiments is known, the calculations could be carried out with the same convolution factor. In that manner the ratio between the integrated diffuse intensity and the integrated Bragg peak intensities could be used for a comparison with experimental intensities.

I emphasize that the convolution factor does not affect the qualitative shape of the scattering discussed in sections III A - III C, but has to be considered when studying the quantitative defect size effects, section III D.

Unless otherwise mentioned, the calculations in this paper have been carried out using  $\sigma = 0.1$ , which was about the smallest value for which no artificial truncation ripples<sup>19</sup> were observed anywhere in the scattering patterns for the 600 Å diameter atom spheres.

### B. 311 defect structures

In this work, I used defect coordinates calculated by Parisini and Bourret<sup>11</sup> as the seed defect configuration in the calculations. I focused on two configurations, the “IRD” and “1HexZD” defects, which were shown to be the lowest-energy one within the model used, and agree well with experimental observations on 311 defects<sup>20,11</sup>. The nature of these defects is illustrated schematically in Fig. 1 (for an atomic picture, see Ref. 11). In the figure, the thick dashed line indicates where the interstitial atoms are in the core of the defect. The other lines indicate the crystal directions in and perpendicular to the defect plane. In the IRD defect, the interstitial atoms lie in a single (113) crystal plane. In the 1HexZD defect the extra atoms lie in a zig-zag pattern, with interstitial atoms alternately on (113) and ( $\bar{1}\bar{1}\bar{3}$ ) planes. The net effect then is that the 1HexZD plane on average is perpendicular to a  $\langle 100 \rangle$  crystal direction. In both cases, the defect “length” direction is a  $\langle 110 \rangle$  direction, whereas the “width” directions are different. The thickness of the atom plane with interstitials is only a few atom planes.

The 311 cells of Parisini and Bourret have lengths of only about 4 Å, and widths of 30 Å (1HexZD) and 50 Å (IRD). In their modeling, the defects were repeated periodically to infinity. In this study, I repeated the seed cells periodically a finite number of times to obtain different widths  $w$  and lengths  $l$  of the defect. This gave seed cells of varying sizes, which were then embedded into perfect Si crystal as usual in the x-ray calculation. This way, the model describes realistically real finite-sized 311 defects. The embedding was done in such a way that no atoms in the 311 defect plane initially came unrealistically close to atoms in the surrounding

perfect lattice. The conjugate gradient energy relaxation then moved the atoms to the closest minimum. I also performed MD annealing at 600 K on one cell, which did reduce the number of coordination defects at the edges of the 311 defect. However, the effect on the x-ray scattering pattern was negligible.

In reality, the 311 defects are not necessarily perfect, but may contain defects and impurities in their structure. At high concentrations these defects in the 311 defect could affect the scattering pattern, but I do not explore this issue in the present paper.

## III. RESULTS

In the following, I always use unitless Miller indices (“ $hkl$ ”) notation to present the results. Since carrying out an exhaustive search of reciprocal space would be prohibitively expensive computationally, I focus on a few Bragg peaks and planes in reciprocal space, which are frequently studied in experiments as well.

To give an impression of the overall scattering pattern, I illustrate in Fig. 2 a) and b) the scattering from an IRD and 1HexZD defects, both with a size of about  $100 \times 100$  Å<sup>2</sup>. It is readily apparent that there is significant structure in the scattering outside the Bragg peaks, with pronounced streak-like features. I next discuss in detail the scattering patterns emanating from these two defects. I focus on the 111 peak, but also mention features around other peaks.

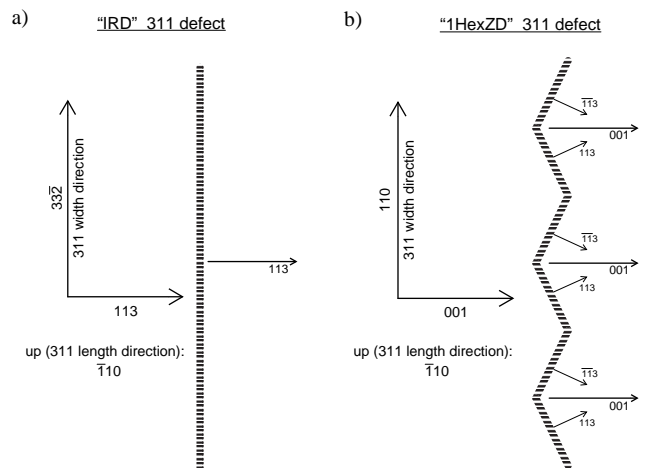


FIG. 1. Schematic illustration of the orientation of the planes containing interstitial atoms in 311 defects. The plane where the extra atoms lie is indicated by thick, dashed lines. The vectors and numbers show crystal directions and their Miller indices. The defect names and the orientation information is from Ref. 11. a) IRD defect, b) 1HexZD defect.

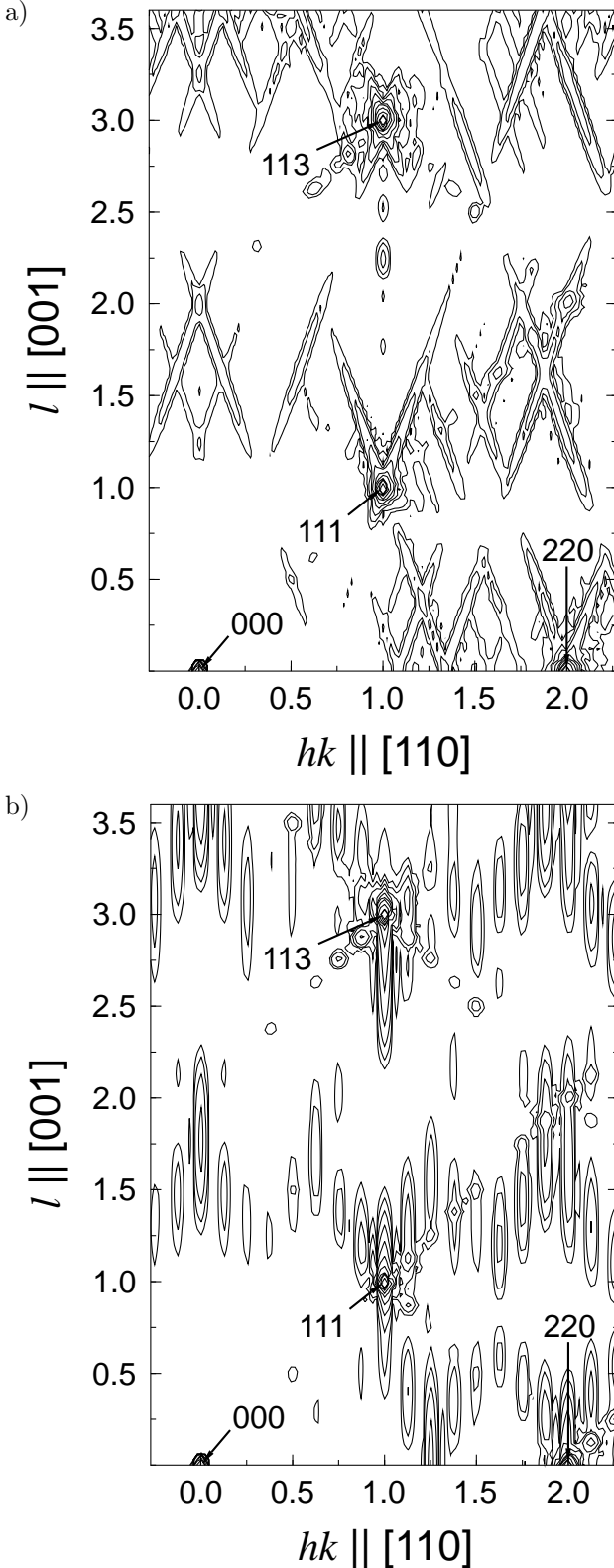


FIG. 2. X-ray scattering pattern of 311 defects of width 100 Å and length 100 Å. The lines are iso-intensity curves, so that 2 curves indicate a difference of one order of magnitude in scattering intensity. The figure shows the plane spanned by the [110] and [001] crystal directions. Also indicated by arrows and numbers are the locations of Bragg peaks. a) IRD defect, b) 1HexZD defect.

Figure 3 a) illustrates the X-ray scattering near the 111 Bragg peak for the IRD defect with a width and length of almost exactly 100 Å. There are two strong streaks emanating from the 111 Bragg peak, one in the [113] direction, the other in the  $[\bar{1}\bar{1}3]$  direction. The reason to the presence of these streaks can be understood by comparing with the x-ray scattering from stacking faults in Si. In an interstitial-like stacking fault, the fault plane produces a discontinuity in the lattice in a [111] direction. This is experimentally known to produce streaks in the x-ray scattering pattern in  $\langle 111 \rangle$  directions, a feature which is correctly reproduced by numerical models and our simulations<sup>6,8</sup>. This can be understood as an analogical effect to the “crystal truncation rods” produced by surfaces, where there also is a discontinuity in the lattice<sup>21</sup>. Moreover, the streaks from stacking faults can be asymmetric, i.e. the streak in the  $\langle 111 \rangle$  need not equal that in the  $\langle \bar{1}\bar{1}\bar{1} \rangle$  direction<sup>8</sup>. In the IRD configuration there is a discontinuity in the lattice in a  $\{311\}$  plane (see Fig. 1 a). Hence both the origin of the asymmetric  $\langle 113 \rangle$  streaks, and their asymmetry, can be understood with analogy to the production of the streaks from stacking faults.

There also seem to be weak, secondary streaks outside the Bragg peak, and repetitive weak peaks in the 111 direction off from the 111 Bragg peaks. However, since these would probably be difficult to detect experimentally due to their low intensity, I do not analyze them in more detail. Moreover, for the weakest features visible in the patterns I can not rule out that numerical problems affect the results. But all the patterns discussed in the text have been verified not to be due to numerical inaccuracies.

I also observed similar  $\langle 113 \rangle$  streaks emanating from other Bragg peaks. The 220 peak was observed to have streaks in all  $\langle 113 \rangle$  directions lying in the plane spanned by the [001] and [110] directions, whereas the 311 peak itself did not have very well-defined streaks, at least for this small 311 defects.

## B. 1HexZD

Figure 3 b) illustrates the X-ray scattering around the 111 peak for the 1HexZD configuration with a width of 92 Å and length of almost exactly 100 Å. Several interesting features in the scattering pattern are evident from the figure. First, there is a strong streak emanating from the 111 peak in the [001] and  $[00\bar{1}]$  directions. Similarly to the IRD defect, the reason for the existence of this streak can be understood by considering Fig. 1 b). The average plane of the 1HexZD defect is a  $\langle 100 \rangle$  direction, and hence the discontinuity of the crystal in this direction can give rise to a streak, as for the IRD 311 defect and the stacking fault<sup>6</sup>. There are no visible streaks in  $\langle 311 \rangle$  directions in this case. Although these directions do play a role in the zig-zag pattern of the 1HexZD defect, the distance between two segments in the zig-zag pattern is so short (about 15 Å) that the possible streak effect appears to cancel efficiently.

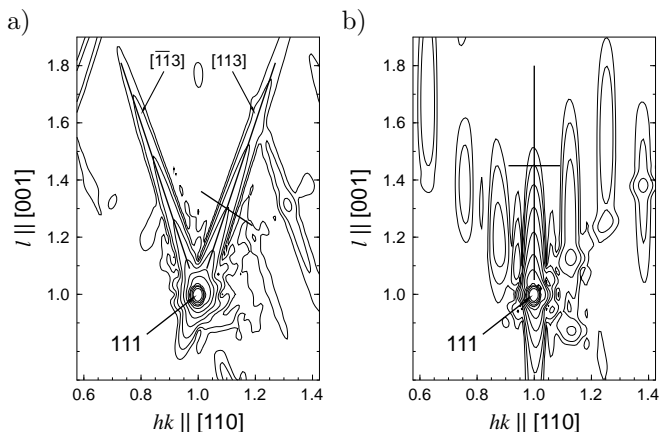


FIG. 3. X-ray scattering pattern of 311 defects of width 100 Å and length 100 Å around the 111 Bragg peak. The lines are iso-intensity curves, so that 2 curves indicate a difference of one order of magnitude in scattering intensity. The figure shows the plane spanned by the [110] (x axis in figure) and [001] (y axis) crystal directions. Also indicated by thick lines are the directions of the main streaks, as well as the scan directions giving the defect widths. a) IRD defect, b) 1HexZD defect.

Secondly, there seem to be weaker streaks also in the 001 direction, parallel to the main streak but separated from it by about  $0.21 \text{ 1/Å}$  along [110] in reciprocal space. I believe this is due to the regular repetition of the zig-zag pattern in the [110] direction of the defect (cf. Fig. 1 b)). The distance between the streaks corresponds to a distance of  $2\pi/(0.21 \text{ 1/Å}) = 30 \text{ Å}$ , which matches almost perfectly the repetition distance of  $31 \text{ Å}$  in the atomic configuration. Moreover, these secondary streaks are not visible in simulation of zig-zag defects with no repetition of the pattern.

Several other peaks also had streaks in some {001} direction. The 311 peak had a strong streak in the  $[00\bar{1}]$  direction, see Fig. 2 b), as did the 333 peak. The 220 peak has streaks in both the [001] and  $[00\bar{1}]$  directions.

Similarly to the IRD defect, the Bragg peaks of the 1HexZD defect cells also have secondary peaks along the 111 direction, but these are again weaker in intensity than the streaks.

### C. Scattering around (1.3 1.3 0)

I also observe a local maximum around  $(1.25 \ 1.25 \ 0) - (1.3 \ 1.3 \ 0)$  in reciprocal space for both types of 311 defects (see Fig. 2). This peak is very close to the peak at about  $(1.2 \ 1.2 \ 0)$  observed in electron diffraction experiments, which has been recognized as the (0002) hexagonal Bragg peak due to a single layer of hexagonal silicon at the center of the defect<sup>20</sup>. It appears that the peak I observe is slightly higher in reciprocal space, which is likely to be related to compressive strain in the core of the defect. Since the experimental peak is lower, it appears the atomistic model overestimates this strain.

The shape of the scattering is quite different for the two types of defects, see Fig. 4, so in principle this region of reciprocal space could also be used to distinguish between

the two types of defects. Even if the fine structure can not be measured, this region may be useful for detecting whether any 311 defects are present in the sample.

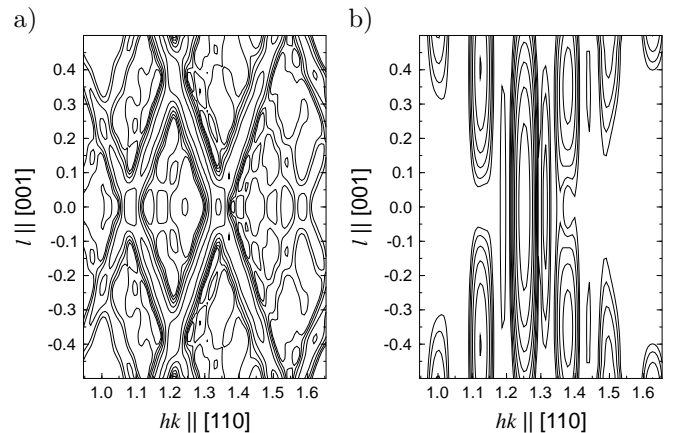


FIG. 4. X-ray scattering pattern of 311 defects of width 100 Å and length 100 Å around  $(1.3 \ 1.3 \ 0)$  in reciprocal space. The lines are iso-intensity curves, so that 4 curves indicate a difference of one order of magnitude in scattering intensity. The figure shows the plane spanned by the [110] (x axis in figure) and [001] (y axis) crystal directions. a) IRD defect, b) 1HexZD defect.

### D. Defect width and length effects

I also performed systematic simulations of IRD and 1HexZD defects of sizes ranging from  $30 \text{ Å}$  to  $150 \text{ Å}$  in width and length to examine size effects on the scattering.

For the IRD defect, I found that the *width* of the  $\langle 311 \rangle$  streaks is related to the width and length of the defect according to the crystal direction. To be specific, the IRD defect width direction  $[33\bar{2}]$  is reflected in the width of the [113] streak along the  $[33\bar{2}]$  direction in reciprocal space. Similarly, the width of the streak in the  $[\bar{1}10]$  direction is proportional to the length of the defect, which is the  $[\bar{1}10]$  direction. The same dependence was found for 1HexZD for the [001] streaks in directions corresponding to the defect width and length.

A similar size dependence has been previously reported for stacking faults<sup>8</sup>, but this dependence was on the average radius of the defect only and did not distinguish between defect length and width. In the stacking fault work, the streak width in reciprocal space was derived to be simply proportional to the inverse of the defect size in real space. Hence I use the same functional form for the 311 defects.

I first discuss in detail the defect widths. The width dependence is illustrated in Fig. 5 a) for the IRD defect. It shows a cross-sectional scan along the  $[33\bar{2}]$  direction through the [113] streak emanating from the 111 Bragg peaks. The direction of this scan is illustrated in Fig. 3 a). The x axis is given as the unitless distance from  $(1.1 \ 1.1 \ 1.3)$  in reciprocal  $(hkl)$  space. It is readily apparent that the streak width is independent of the defect length  $l$ , but clearly dependent on the defect width  $w$ . The inset shows the full width at half maximum (fwhm) of

the streaks as a function of the defect width. The line is  $\text{fwhm} = 4.96 \text{ \AA}/w$ . Because of the good quality of the fit, it is plausible that this equation can be used to estimate the widths of even much larger IRD-like 311 defects.

The same process was repeated for the 1HexZD defect with a scan along  $[110]$  through the streak, centered at  $(1.0 \ 1.0 \ 1.45)$ , see Fig. 5 b). The direction of this scan is illustrated in Fig. 3 b). Again the streak width is proportional to the defect width, although for the smallest defects there is some variation, probably due to overlap with other features in the scattering. The fit in the inset gives my best fit of  $\text{fwhm} = 4.0 \text{ \AA}/w$ , which does describe quite well the defects with width larger than  $30 \text{ \AA}$ .

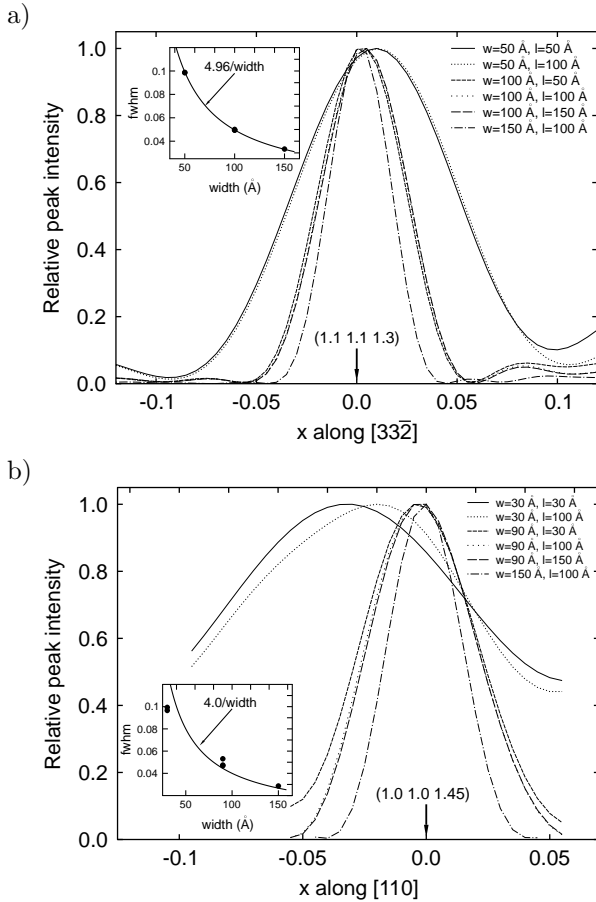


FIG. 5. Dependence of the streak width on the width of 311 defects. The maximum in the scattering intensity is normalized to 1 to allow for easy comparison of the widths. The insets show the fwhm of the intensity peak as a function of the defect width for all the defects studied. a) IRD defect, b) 1HexZD defect.

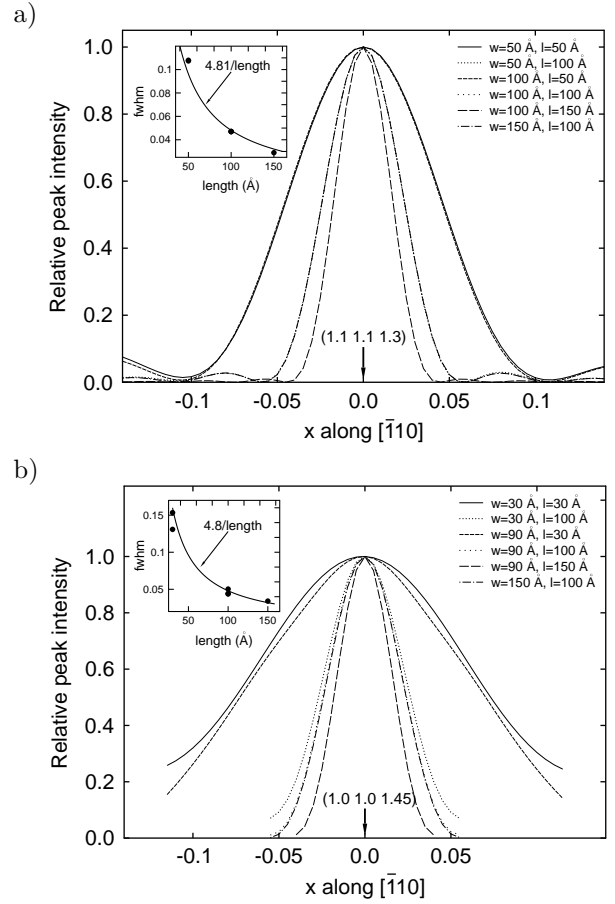


FIG. 6. Dependence of the streak width on the length of 311 defects. The maximum in the scattering intensity is normalized to 1 to allow for easy comparison of the widths. The inset shows the fwhm of the intensity peak as a function of the defect length for all the defects studied. a) IRD defect, b) 1HexZD defect.

The length of the defects behaves very similarly, see Fig. 6. Now the scan is in the  $[\bar{1}10]$  direction for both defects (out of the plane in Fig. 3, and the functional dependence found is  $\text{fwhm} = 4.81 \text{ \AA}/l$  for the IRD defect, and  $4.8 \text{ \AA}/l$  for the 1HexZD defect. The fit is again very good for the IRD defect, but somewhat poorer for the 1HexZD defect.

I did not report the statistical uncertainty of the fits because the main source of uncertainty here is systematic errors the  $\sigma$  convolution factor. The influence of the  $\sigma$  factor was assessed by repeating some of the calculations described above as a function of  $\sigma$ , for  $\sigma$  values in the range  $0.05 - 0.30$ . These tests showed that both the width and the length do depend on sigma, but in a fairly smooth manner, enabling interpolation or extrapolation to any value of  $\sigma \lesssim 0.3$ . I estimated that for  $\sigma \lesssim 0.10$  (the range likely to be relevant for experiments) the effect is not more than roughly 30%. Hence the size dependencies presented above are valid for a first estimate of defect size. A more accurate estimate can be obtained by carrying out the modeling for a  $\sigma$  value corresponding to the experimental resolution of a given set of experiments.

As an aside, I note that for stacking faults we have previously found the dependence  $\text{fwhm} = 6.8 \text{ \AA}/\text{diameter}^6$ ,

so the streak width dependence of the defect size seems to be of the same order of magnitude for many different kinds of defects. Moreover, this dependence agreed with independent analytical calculations<sup>22</sup>, giving additional confidence that the  $\sigma$  parameter at most causes a minor correction in the dependence.

#### IV. CONCLUSIONS

Using an atomistic scheme to calculate the diffuse x-ray scattering, I have shown what the expected scattering pattern for the two most common 311 defects is expected to look like. The “IRD” variety has pronounced streaks in  $\langle 311 \rangle$  directions, while the “1HexZD” variety has streaks in  $\langle 100 \rangle$  directions in reciprocal space. Moreover, I showed how cross-sectional scans of these streaks could be used to determine approximately the defect width and length separately, and discussed how the first approximation presented here could be made more accurate in connection with experiments.

Since a stacking fault has streaks in  $\langle 111 \rangle$  directions, and the perfect loop no streaks, our results mean that using x-rays the two varieties of the 311 defect could be distinguished both from each other, and the other important extended defects which play a role in Si processing.

#### ACKNOWLEDGMENTS

I am grateful to Dr. A. Parisini and Prof. A. Bourret for useful discussions, and providing the atom coordinates of their 311 defect models. I also thank Dr. T. H. Metzger, Dr D. Lübbert and Dr. J. Patel for input on experimental issues, and Dr. P. Ehrhart for enlightening comments on the role of the convolution factor in the calculations. The research was supported by the Academy of Finland under project No. 44215. Grants of computer time from the Center for Scientific Computing in Espoo, Finland are gratefully acknowledged.

- <sup>7</sup> P. H. Dederichs, J. Phys. F: Metal Phys. **3**, 471 (1973).
- <sup>8</sup> P. Ehrhart, H. Trinkaus, and B. C. Larson, Phys. Rev. B **25**, 834 (1982).
- <sup>9</sup> S. Takeda, S. Muto, and M. Hirata, Jap. J. Appl. Phys. **29**, L1698 (1990).
- <sup>10</sup> S. Takeda, Jap. J. Appl. Phys. **30**, L639 (1991).
- <sup>11</sup> A. Parisini and A. Bourret, Phil. Mag. A **67**, 605 (1992).
- <sup>12</sup> D. J. Eaglesham, P. A. Stolk, H.-J. Gossmann, T. E. Haynes, and J. M. Poate, Nucl. Instr. Meth. Phys. Res. B **106**, 191 (1995).
- <sup>13</sup> R. Raman, M. E. Law, V. Krishnamoorthy, and K. S. Jones, Appl. Phys. Lett. **74**, 700 (1999).
- <sup>14</sup> K. Nordlund, P. Partyka, and R. S. Averback, in *Defects and Diffusion in Silicon Processing*, Vol. 469 of *MRS Symposium Proceedings*, edited by T. Diaz de la Rubia, S. Coffa, P. A. Stolk, and C. S. Rafferty (Materials Research Society, Pittsburgh, 1997), pp. 199–204.
- <sup>15</sup> K. Nordlund, P. Partyka, R. S. Averback, I. K. Robinson, and P. Ehrhart, J. Appl. Phys. **88**, 2278 (2000).
- <sup>16</sup> P. Partyka, Y. Zhong, K. Nordlund, R. S. Averback, I. K. Robinson, and P. Ehrhart, Phys. Rev. B **64**, 235207 (2002).
- <sup>17</sup> F. H. Stillinger and T. A. Weber, Phys. Rev. B **31**, 5262 (1985).
- <sup>18</sup> J. Tersoff, Phys. Rev. B **38**, 9902 (1988).
- <sup>19</sup> D. T. Keating and A. N. Goland, Acta Cryst. A **27**, 134 (1971).
- <sup>20</sup> A. Bourret, in *Microsc. Semicond. Mater. Conf.*, No. 87 in *Inst. Phys. Conf. Ser.*, edited by A. G. Cullis and P. D. Augustus (IOP publishing, ADDRESS, 1987).
- <sup>21</sup> I. K. Robinson and D. J. Tweet, Reports on Progress in Physics **55**, 599 (1992).
- <sup>22</sup> V. Holy, private communication.

---

<sup>1</sup> E. Chason *et al.*, J. Appl. Phys **81**, 6513 (1997), and references therein.

<sup>2</sup> P. Ehrhart, J. Nucl. Mater. **216**, 170 (1994).

<sup>3</sup> S. Grotehans, G. Wallner, E. Burkel, H. Metzger, J. Peisl, and H. Wagner, Phys. Rev. B **39**, 8450 (1989).

<sup>4</sup> P. Ehrhart and H. Zillgen, in *Defects and Diffusion in Silicon Processing*, Vol. 469 of *MRS Symposium Proceedings*, edited by T. Diaz de la Rubia, S. Coffa, P. A. Stolk, and C. S. Rafferty (Materials Research Society, Pittsburgh, 1997), p. 175.

<sup>5</sup> P. Partyka, R. S. Averback, D. V. Forbes, J. J. Coleman, and P. Ehrhart, J. Appl. Phys. **83**, 1265 (1998).

<sup>6</sup> K. Nordlund, U. Beck, T. H. Metzger, and J. R. Patel, Appl. Phys. Lett. **76**, 846 (2000).